

# Collision-Free Flocking with a Dynamic Squad of Fixed-Wing UAVs Using Deep Reinforcement Learning

Chao Yan, Xiaojia Xiang, Chang Wang\*, and Zhen Lan

**Abstract**—Developing the collision-free flocking behavior for a dynamic squad of fixed-wing UAVs is still a challenge due to kinematic complexity and environmental uncertainty. In this paper, we deal with the decentralized leader-follower flocking control problem through deep reinforcement learning (DRL). Specifically, we formulate a decentralized DRL-based decision making framework from the perspective of every follower, where a collision avoidance mechanism is integrated into the flocking controller. Then, we propose a novel reinforcement learning algorithm CACER-II for training a shared control policy for all the followers. Besides, we design a plug-n-play embedding module based on convolutional neural networks and the attention mechanism. As a result, the variable-length system state can be encoded into a fixed-length embedding vector, which makes the learned DRL policies independent with the number or the order of followers. Finally, numerical simulation results demonstrate the effectiveness of the proposed method, and the learned policies can be directly transferred to semi-physical simulation without any parameter finetuning.

## I. INTRODUCTION

Due to the capability limitation of a single unmanned aerial vehicle (UAV), multi-UAV collaboration has attracted increasing attention [1], [2]. One of the fundamental and challenging problems is the flocking control of UAVs without collision [3]. Traditional methods such as model predictive control [4] and consensus theory [5] usually depend on precise physical models, which are complex and difficult to obtain in practice. As an alternative, reinforcement learning (RL) [6], [7] can be used for the flocking control problem. For example, Hung et al. used the Dyna-Q( $\lambda$ ) algorithm [8] and the Q( $\lambda$ ) algorithm [9] to learn flocking control policies for fixed-wing UAVs. Speck et al. [10] combined the SARSA algorithm with object-focused learning to implement the formation control of a UAV swarm in a distributed manner. However, the above methods simplified the problem by discretizing the state and action spaces, which was inappropriate for controlling the UAVs in more realistic environments. Besides, the collision avoidance problem was also simplified by assuming the UAVs were at different fixed-altitudes.

Deep reinforcement learning (DRL) has been proved effective for high-dimensional and continuous control problems in robotics [11], [12], [13]. In our previous work, we proposed a DRL algorithm, i.e., continuous actor-critic with experience replay (CACER), for flocking with fixed-wing UAVs in continuous state and action spaces [14], [15]. Following the

This work was supported by National Natural Science Foundation of China (61906203).

College of Intelligence Science and Technology, National University of Defense Technology, Changsha 410073, China, {yancho17, xiangxiaoja, wangchang07, lanzhen19} @nudt.edu.cn \*Corresponding author

previous work [8], [9], we also simplified the collision avoidance problem by assuming that the UAVs maintained the same constant speed but different altitudes. However, some real-world applications such as surveying and mapping require the UAVs to flock at the same altitude. This requirement makes flocking control more challenging, because the collision avoidance problem must be considered. In contrast to the previous work [8], [9], [14], this paper relaxes the above assumptions and solves a more challenging leader-follower flocking control problem. Specifically, we not only allow the UAVs to change speed as needed, but also design a collision avoidance mechanism and integrate it into the flocking controller.

Besides, it is difficult to construct a collision-free leader-follower flocking control model for a dynamic squad of UAVs. The main reason is that the length of the system state is relevant with the number of followers, while the DRL-based control policies typically require a fixed-length input for deep neural networks. Sui et al. [16] followed the method in [17] where long short-term memory network (LSTM) [18] was applied to process the states of other followers sequentially in the reverse order of their distances to the decision-making follower, under the assumption that the nearest neighbor had the biggest effect on the follower. However, this assumption is not always true due to the influence of other factors such as speed and heading. Instead, we design a customized network module to deal with the collision avoidance problem for a dynamic squad of fixed-wing UAVs.

The main contributions of this paper are as follows:

- A decentralized DRL-based framework is designed to address the collision-free flocking control problem for a dynamic squad of fixed-wing UAVs.
- A novel DRL algorithm is proposed for training the flocking controller, where a plug-n-play embedding module based on convolutional neural networks and the attention mechanism is designed to handle variable-length system state.
- The proposed method can be directly transferred from numerical simulation to semi-physical simulation without any parameter finetuning.

The rest of this paper is organized as follows. Section II formulates the flocking and collision avoidance problem, followed by the proposed CACER-II algorithm and the designed SEMP embedding module in Section III. Section IV discusses the simulation results. Finally, Section V concludes this paper.

## II. PROBLEM FORMULATION

In this section, we describe the collision-free flocking problem and the kinematics of fixed-wing UAV. Then, we formulate this problem as a Markov decision process (MDP) in an RL framework.

### A. Problem Description

In our flocking scenario, a unique leader is followed by a variable number of followers. These followers are homogeneous and fly at the same altitude[9], [19]. The leader is remotely controlled by a human operator via a ground control station. We assume that each UAV is able to obtain the state of other UAVs through the inner communication channel [20]. Each follower has to select its steering commands independently to maintain a certain distance  $\rho$  from the leader ( $d_1 < \rho < d_2$ ) while avoiding collision with other followers simultaneously, as shown in Figure 1. We note that the followers are allowed to use the same decentralized control policy.

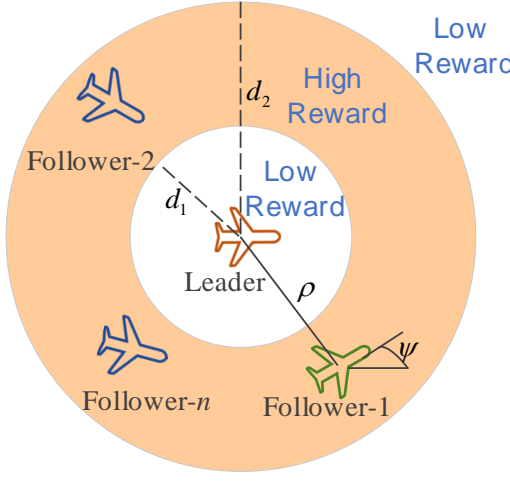


Fig. 1. The top view of the relationship between the leader and followers. Note that the number of followers, i.e.,  $n$ , is a variable.

### B. Kinematics of Fixed-Wing UAVs

In this paper, we follow the numerical kinematic model of fixed-wing UAVs with stochastic disturbances in [14] to generate simulated samples for training the DRL-based control policy. Instead of assuming that the airspeed of the UAV is drawn from a normal distribution with a constant mean, we define the airspeed dynamics to describe the response relationships between the desired airspeed  $v_d$  and the actual airspeed  $v$ , similar to the roll dynamics that describes the response relationships between the roll-angle setpoint  $\phi_d$  and the actual roll-angle  $\phi$  in [14]. Besides, we also simulate the initial condition responses of the airspeed dynamics based on a second-order system, and additionally introduce the stochasticity to make the simulation more realistic. The parameters of the second-order system, i.e., the undamped natural frequency  $\omega_n^v$  and the damping ratio  $\zeta_v$ , are drawn

from the normal distributions  $(\bar{\omega}_n^v, \sigma_{\omega_n^v}^2)$  and  $(\bar{\zeta}_v, \sigma_{\zeta_v}^2)$ , respectively. We rewrite the extended kinematics as follows:

$$\dot{\xi} = \frac{d}{dt} \begin{Bmatrix} x \\ y \\ \psi \\ \phi \\ v \end{Bmatrix} = \begin{Bmatrix} v \cos \psi + \eta_x \\ v \sin \psi + \eta_y \\ -(\alpha_g/v) \tan \phi + \eta_\psi \\ f(\phi, \phi_d) \\ f(v, v_d) \end{Bmatrix}. \quad (1)$$

where  $(x, y)$  is the planar position;  $\psi$  is the heading angle;  $\phi$  is the roll-angle;  $v$  is the airspeed;  $\alpha_g$  is the gravitational acceleration;  $(\eta_x, \eta_y, \eta_\psi)$  are disturbance terms that follow normal distributions;  $f(\phi, \phi_d)$  and  $f(v, v_d)$  denote the functions that describe the roll dynamics and the airspeed dynamics, respectively.

### C. MDP of Collision-Free Flocking

1) *State Representation*: As mentioned above, there are one leader and  $n$  followers. From the perspective of an arbitrary follower, e.g., follower- $i$  ( $i = 1, 2, \dots, n$ ), the flock of UAVs can be divided into three groups: the follower- $i$  itself (termed as the *ego-follower*), the leader, and the other followers  $\{\text{follower-}j \mid j = 1, 2, \dots, n, j \neq i\}$ . Accordingly, the system state is composed of three parts: the ego-follower's state  $\xi_e = \xi_f^i$ , the leader's state  $\xi_l$ , and the other followers' states  $\xi_o = \{\xi_f^j \mid j = 1, 2, \dots, n, j \neq i\}$ , where  $\xi := (x, y, \psi, \phi, v)$  is a tuple that describes the state of a single fixed-wing UAV according to its kinematics.

To reduce the redundancy of the representation of the system state [21], the *ego-follower and leader joint state*  $s^e := (s_1^e, s_2^e, s_3^e, s_4^e, s_5^e, s_6^e, s_7^e, s_8^e, s_9^e)$  is defined as:

$$\left\{ \begin{array}{l} \begin{bmatrix} s_1^e \\ s_2^e \end{bmatrix} = \begin{bmatrix} \cos \psi_l & \sin \psi_l \\ -\sin \psi_l & \cos \psi_l \end{bmatrix} \begin{bmatrix} x_e - x_l \\ y_e - y_l \end{bmatrix} \\ s_3^e = \psi_e - \psi_l \\ s_4^e = \phi_e \\ s_5^e = \phi_l \\ s_6^e = \phi_d^l \\ s_7^e = v_e \\ s_8^e = v_l \\ s_9^e = v_d^l \end{array} \right. , \quad (2)$$

where  $(s_1^e, s_2^e)$  is the planar position of the ego-follower relative to the leader;  $s_3^e$  is the difference in the heading between the leader and the follower. Besides,  $\phi_d^l$  and  $v_d^l$  are the roll-angle and velocity setpoints of the leader, respectively.

The *ego-follower and other followers joint state*  $s^o = \{s_j^o := (s_{1,j}^o, s_{2,j}^o, s_{3,j}^o, s_{4,j}^o, s_{5,j}^o) \mid j = 1, 2, \dots, n, j \neq i\}$  is defined as:

$$\left\{ \begin{array}{l} \begin{bmatrix} s_{1,j}^o \\ s_{2,j}^o \end{bmatrix} = \begin{bmatrix} \cos \psi_f^j & \sin \psi_f^j \\ -\sin \psi_f^j & \cos \psi_f^j \end{bmatrix} \begin{bmatrix} x_f^j - x_e \\ y_f^j - y_e \end{bmatrix} \\ s_{3,j}^o = \psi_f^j - \psi_e \\ s_{4,j}^o = \phi_f^j \\ s_{5,j}^o = v_f^j \end{array} \right. , \quad (3)$$

where  $(s_{1,j}^o, s_{2,j}^o)$  represents the planar position of another follower- $j$ , relative to the ego-follower;  $s_{3,j}^o$  denotes the difference in the heading between the ego-follower and follower- $j$ .

Consequently, concatenating the two joint states above, we construct the state representation of the system  $s := (s^e, s^o)$ . We note that its dimensionality depends on the number of followers.

2) *Action Space*: The followers are maneuvered by executing the roll and velocity actions. In this paper, we define the action  $a := (a_r, a_v)$  in continuous spaces, where the roll action  $a_r \in [-10^\circ, +10^\circ]$  and the velocity action  $a_v \in [-1, +1]$ . The current roll-angle and airspeed of a follower are denoted by  $\phi$  and  $v$ , respectively. The next roll-angle setpoint  $\phi_d$  can be calculated by:

$$\phi_d = \begin{cases} r_{bd} & \text{if } \phi + a_r > r_{bd} \\ -r_{bd} & \text{if } \phi + a_r < -r_{bd} \\ \phi + a_r & \text{otherwise} \end{cases}, \quad (4)$$

where  $[-r_{bd}, r_{bd}]$  is the allowed range of the roll-angle setpoint.

Similarly, the next velocity setpoint  $v_d$  is defined by:

$$v_d = \begin{cases} v_{\max} & \text{if } v + a_v > v_{\max} \\ v_{\min} & \text{if } v + a_v < v_{\min} \\ v + a_v & \text{otherwise} \end{cases}, \quad (5)$$

where the  $v_{\max}$  and  $v_{\min}$  denote the maximum velocity and the minimum velocity of the follower, respectively.

3) *Reward Function*: In this paper, the followers aim to avoid collision between each other while flocking with the leader. Therefore, the reward function consists of two pieces: the *flocking reward* and the *collision penalty*. Specifically, in order to facilitate the agent (i.e., the ego-follower) to maintain a suitable distance from the leader, the *flocking reward*  $r_l$  is designed as follows:

$$\begin{cases} r_l = -\max \left\{ d_e, \frac{d_1 |s_3^e|}{\pi(1+\omega d_e)} \right\} \\ d_e = \max \{m(d_1 - \rho), 0, \rho - d_2\} \\ \rho = \sqrt{|s_1^e|^2 + |s_2^e|^2} \end{cases}, \quad (6)$$

where  $d_1$  and  $d_2$  are the inner and outer radius of an annulus shown in Figure 1, respectively.  $d_e$  indicates the distance from the agent to this annulus, and  $\rho$  denotes the distance between the leader and the agent. Both  $\omega$  and  $m$  are tuning parameters. Besides, the *collision penalty*  $r_c^j$  is defined to prevent the agent from colliding with the follower- $j$ , as follows:

$$\begin{cases} r_c^j = -\max \{m(d_1 - \rho_j^o), 0\} \\ \rho_j^o = \sqrt{|s_{1,j}^o|^2 + |s_{2,j}^o|^2} \end{cases}, \quad (7)$$

where  $\rho_j^o$  is the distance from the agent to follower- $j$ .

Lastly, the final reward function  $r$  is specified as:

$$r = r_l + \sum_j r_c^j. \quad (8)$$

### III. APPROACH

#### A. CACER-II

In our previous work [14], [15], we proposed an algorithm called continuous actor-critic with experience replay (CACER). In contrast to other actor-critic algorithms, e.g., DDPG [22], one distinctive feature of CACER is in its positive-temporal difference (TD) update scheme [23] for training the policy (actor). In other words, the CACER algorithm updates its policy only when the TD-error is positive [24]. In this paper, we propose a novel algorithm CACER-II by extending CACER to a multi-agent scenario (see Algorithm 1).

As mentioned in Section II-A, all the followers are allowed to share the same policy. This shared policy can be optimized more efficiently with the data of experiences collected by all the followers. We note that the CACER-II algorithm follows the *centralized-learning and decentralized-execution* fashion [25]. In other words, during the learning phase, experiences obtained by all the followers simultaneously are stored into a shared experience replay memory, and the shared policy in terms of deep neural networks are trained with the stored experiences centrally (centralized-learning). Nevertheless, during the execution phase, each follower independently selects and executes its action by following the shared policy based on its perceived state (decentralized-execution).

#### B. Network Architecture

In accordance with the similar actor-critic approaches, we use deep neural networks to approximate the actor and the critic, respectively. Inspired by [26] and [27], we design a customized network module based on convolutional neural networks and attention mechanisms, which makes our algorithm can adapt to the changes of the number of followers.

As illustrated in Figure 2, the Embedding module is composed of two convolutional layers (Conv), two *Squeeze-and-Excitation* (SE) blocks [27], a permute layer (Permute), a max-pooling layer (MaxPooling), and a flatten layer (Flatten). First, the variable-length input (i.e., the *ego-follower and other followers joint state*  $s^o$ ) is passed by two convolutional layers (i.e., Conv1 and Conv2) successively. The filter size of Conv1 is equal to the length of  $s_j^o$ , while the filter size of Conv2 is equal to the number of filters of Conv1. With this specialized structure, each feature map extracted by convolutional layers only depends on one follower (one of the other followers). Besides, benefitting from the properties of CNNs, i.e., weight sharing and shift invariance [27], the sequencing operations according to the distances between the leader and the followers as in [17] are no longer required. In other words, the output are invariant to the indexing of the followers.

After each convolutional layer, a SE block is added to improve the capacity for feature extraction of networks. The SE block is a channel attention mechanism. Each SE block uses a global average pooling layer (GlobalAvePooling) in the *squeeze* phase and two fully-connected layers (Dense)

---

**Algorithm 1** CACER-II

---

**Input:**  $N_s$  – maximum time steps;  $N_b$  – training batch size;  $M$  – desired number of training episodes

- 1: Empty replay memory  $D$  with capacity  $N$
- 2: Initialize actor  $Act(s|\theta^A)$  and critic  $V(s|\theta^V)$  randomly
- 3: **for** episode = 1 to  $M$  **do**
- 4:   Initialize the number of followers  $n$ , the leader's state  $\xi_l$ , and the states of followers randomly
- 5:   Initialize the leader's roll-angle setpoint  $\phi_d^l$  and the velocity setpoint  $v_d^l$  randomly
- 6:   **for** follower- $i$  = 1 to  $n$  **do**
- 7:     Observe the leader's state  $\xi_l$ , the states of the other followers  $\xi_o$ , and its own state  $\xi_e$
- 8:     Create the system state  $s_i$  using (2) and (3)
- 9:   **end for**
- 10:   **for**  $t$  = 1 to  $N_s$  **do**
- 11:     **for** follower- $i$  = 1 to  $n$  **do**
- 12:       Select the action  $a_i$  from a Gaussian distribution centered around the output of the actor network taking  $s_i$  as input
- 13:       Calculate the roll-angle setpoint  $\phi_d^f$  and the velocity setpoint  $v_d^f$  according to (4) and (5)
- 14:        $\xi'_e \leftarrow \text{UAV Kinematics}(\xi_e, \phi_d^f, v_d^f)$
- 15:     **end for**
- 16:      $\xi'_l \leftarrow \text{UAV Kinematics}(\xi_l, \phi_d^l, v_d^l)$
- 17:     Select the leader's roll and velocity actions randomly
- 18:     Calculate the leader's next roll-angle setpoint  $\phi_d'^l$  and its next velocity setpoint  $v_d'^l$  using (4) and (5)
- 19:     **for** follower- $i$  = 1 to  $n$  **do**
- 20:       Observe the leader's state  $\xi'_l$ , the states of the other followers  $\xi'_o$ , and its own state  $\xi'_e$
- 21:       Create subsequent system state  $s'_i$  by (2) and (3)
- 22:       Calculate the immediate reward  $r_i$  using (8)
- 23:       Store the state transition tuple  $(s_i, a_i, r_i, s'_i)$  in  $D$ , and replace the oldest tuple if  $\|D\| > N$
- 24:        $s_i \leftarrow s'_i$
- 25:     **end for**
- 26:      $(\phi_d^l, v_d^l) \leftarrow (\phi_d'^l, v_d'^l)$
- 27:     Sample a mini-batch of  $N_b$  tuples  $(s_k, a_k, r_k, s'_k)$  ( $k = 1, 2, \dots, N_b$ ) from  $D$  uniformly
- 28:     Empty the temporal buffer  $D' = \emptyset$
- 29:     **for** tuple  $k$  = 1 to  $N_b$  **do**
- 30:       Calculate TD-error  $\delta_k = r_k + \gamma \cdot V(s'_k|\theta^V) - V(s_k|\theta^V)$
- 31:       Save the tuple  $k$  to  $D'$  if  $\delta_k > 0$
- 32:     **end for**
- 33:     Update the parameter of the actor network  $\theta^A$  with the loss of  $\frac{1}{\|D'\|} \sum_{k'} \|a_{k'} - Act(s_{k'}|\theta^A)\|^2$
- 34:     Update the parameter of the critic network  $\theta^V$  with the loss of  $\frac{1}{N_b} \sum_k \|\delta_k\|^2$
- 35:   **end for**
- 36: **end for**

---

with different activation functions in *excitation* phase, followed by a channel-wise scaling operation (Multiply). By explicitly modelling the relationship between channels, this architectural unit can enhance its selectivity to the more informative features while suppressing the less useful ones, boosting the representational power of the network [27]. After the second Multiply layer, a max-pooling layer is added to create a fixed-size output, independent of the input order and length. Lastly, the output of the max-pooling

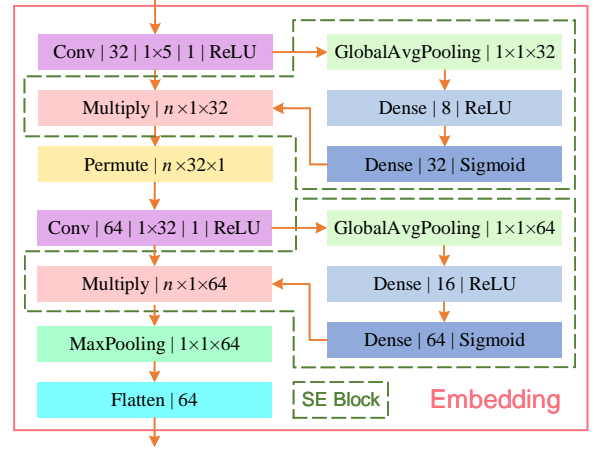


Fig. 2. Embedding module. Each convolutional layer (Conv) is featured by the number of filters, filter size, stride, and activation mode. Other layers are represented by their type/name and output size.

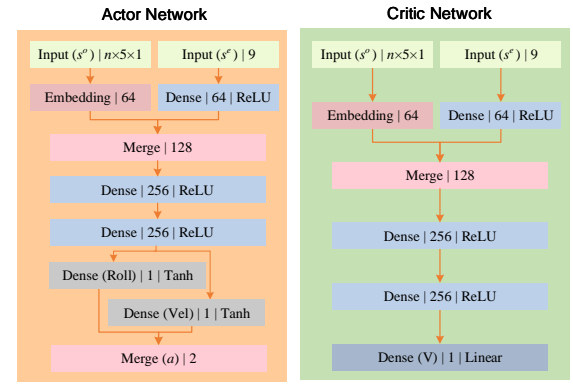


Fig. 3. Network architecture. Each fully-connected layer (Dense) is featured by its type, number of neurons, and activation mode. Other layers are represented by their type/name and output size.

layer is flattened by a flatten layer to create a fixed-length embedding vector. In this way, the variable-length input can be embedded into a fixed-length embedding vector.

We term our scheme of the Embedding module as *SE-MaxPooling* (SEMP). The designed SEMP embedding module can handle inputs with arbitrary length and its output is independent of the input order. We note that this module is plug-n-play, which means the SEMP embedding module can be easily integrated with other network architectures, as well as any reinforcement learning algorithms.

The entire architecture of the actor network and the critic network is depicted in Figure 3. We process the *ego-follower and leader joint state*  $s^e$  and the *ego-follower and other followers joint state*  $s^o$  separately [16]. Specifically, a dense layer with ReLU activation function is used to extract the features of  $s^e$ , and the Embedding module is used to encode the  $s^o$  into a fixed-length vector. After that, the two outputs above are merged and then subsequently fed into 3 dense layers with different activation functions. Note that both the actor and the critic use the same network architecture up

to the last output layer. The output layer of the critic uses a linear activation function, while the output layer of the actor uses a hyperbolic tangent ( $\tanh$ ) activation function.

#### IV. SIMULATION RESULTS

In this section, we evaluate the proposed CACER-II algorithm with the SEMP scheme in both numerical simulation and semi-physical simulation.

##### A. Simulation Setup

In this paper, the CACER-II algorithm was trained with a total of 30000 episodes ( $M = 30000$ ), in which each episode had a maximal number of 60 time steps ( $N_s = 60$ ). All network parameters were updated with 64 batch size ( $N_b = 64$ ), Adam optimizer [28] with 0.001 (for actor) and 0.0001 (for critic) learning rates. The exploration parameter was annealed exponential from 0.5 to 0.05 over a period of 2000 episodes, and then fixed at 0.05 thereafter. In summary, the empirical values of essential parameters are listed in Table I [14], [15].

TABLE I  
PARAMETER SETTINGS

Name	Value	Name	Value
$d_1$	40	$d_2$	65
$\omega$	0.05	$m$	2
$\alpha_g$	9.8	$r_{bd}$	$30^\circ$
$\bar{\omega}_n^v$	5.06	$\sigma_{\omega_v}$	0.5
$\bar{\zeta}_v$	0.75	$\sigma_{\zeta_v}$	0.1
$\bar{\omega}_n^r$	6.3	$\sigma_{\omega_r}$	0.5
$\bar{\zeta}_v$	0.56	$\sigma_{\zeta_r}$	0.1
$\bar{\eta}_x$	0	$\sigma_x$	0.5
$\bar{\eta}_y$	0	$\sigma_y$	0.5
$\bar{\eta}_\psi$	0	$\sigma_\psi$	0.2
$v_{\max}$	18	$v_{\min}$	12
$N$	100000	$\gamma$	0.95

##### B. Numerical Simulation

In order to verify the effectiveness of the proposed SEMP scheme, three existing state-of-the-art approaches, LSTM [17], SA (social attentive pooling) [29], and CNNMP (convolutional neural networks and max pooling)[26], were selected as the benchmarks. To make a fair comparison, we kept their network architectures the same except for the embedding module. Besides, the above solutions also used the same learning algorithm, i.e., the CACER-II algorithm, to update their network parameters. We note that, i) the number of LSTM cells was set to 64, in accordance with the length of the fixed-length vector encoded by SEMP. ii) the network and its parameters used by SA were the same as [29]. iii) The network structure of CNNMP was the same as SEMP, except that SEMP merged a channel attention mechanism by adding two SE blocks.

In the training phase, we evaluate the performance of the proposed algorithm using the *average reward*  $G_{\text{Ave}}$  obtained

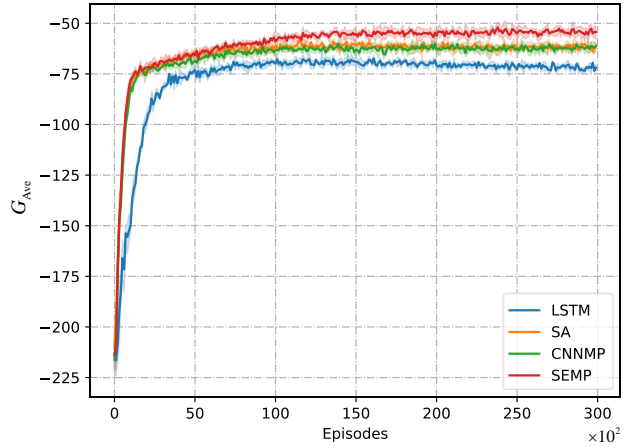


Fig. 4. Learning curves of LSTM, SA, CNNMP, and SEMP.

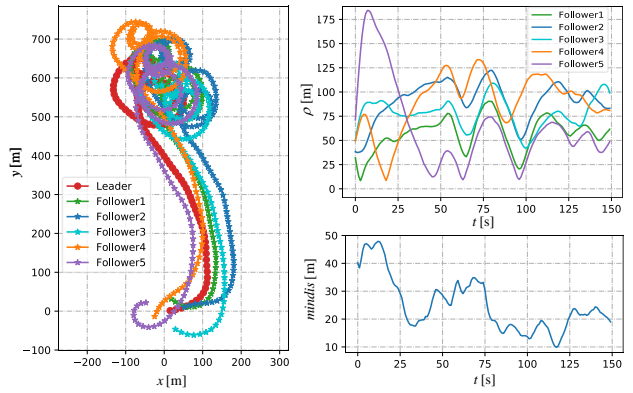


Fig. 5. The visualized results of the five followers following the leader using the learned SEMP policy, i.e., trajectories (left), the distances ( $\rho$ ) to the leader (top-right), and the minimum distance ( $mindis$ ) among the followers (bottom-right).

by one agent within a certain number of  $n_e$  episodes:

$$G_{\text{Ave}} = \frac{1}{n N_e N_s} \sum_{i=1}^n \sum_{p=1}^{N_e} \sum_{t=1}^{N_s} i r_t^p, \quad (9)$$

where  $i r_t^p$  is the immediate reward obtained by agent  $i$  at the time step  $t$  of the episode  $p$  according to (8). Without loss of generality, we set  $N_e = 100$ .

The learning curves of the four above approaches are shown in Figure 4. As can be seen, the LSTM scheme has the worst performance in terms of both learning efficiency and the obtained average reward. Besides, the learning curves of SA and CNNMP are almost overlapped, indicating that the two schemes have similar performance. Additionally, the average reward obtained by SEMP grows as fast as CNNMP in the early stage. However, with the increase of training episodes, the average reward of SEMP still gradually increases, and finally obtains a higher reward. This comparison results validate that the attention mechanism

TABLE II  
COMPARISON RESULTS OF LSTM, SA, CNNMP, AND SEMP

Method	Reward [Ave / Var]				Collision rate (%) [Ave / Var]			
	$n = 4$	$n = 6$	$n = 8$	$n = 10$	$n = 4$	$n = 6$	$n = 8$	$n = 10$
LSTM [17]	-70.99 / 330.43	-76.07 / 292.45	-81.89 / 97.87	-92.70 / 152.85	1.06 / 0.31	1.65 / 0.92	2.09 / 0.28	2.58 / 0.53
SA [29]	-49.25 / 97.86	-59.01 / 104.62	-67.20 / 101.59	-79.72 / 155.76	1.60 / 1.34	1.97 / <b>0.58</b>	2.34 / 0.56	3.20 / 0.84
CNNMP [26]	-48.88 / 127.72	-57.51 / 133.02	-63.39 / 112.21	-72.98 / 122.63	1.41 / 0.72	1.77 / 0.76	1.92 / 0.54	2.56 / 0.45
SEMP (Ours)	<b>-36.95 / 58.32</b>	<b>-45.65 / 79.99</b>	<b>-51.91 / 60.34</b>	<b>-60.54 / 49.67</b>	<b>0.96 / 0.20</b>	<b>1.40 / 0.64</b>	<b>1.71 / 0.45</b>	<b>1.97 / 0.33</b>

with SE blocks used by SEMP is effective. Overall, SEMP finally obtains the highest reward with a similar learning efficiency. This result demonstrates that our SEMP scheme has advantage over the three benchmarks.

After training, we tested the control policy learned by the CACER-II algorithm with the SEMP scheme (hereafter referred to as the learned SEMP policy for short) in a flocking task with five followers lasting for 150 seconds. The testing results are visualized in Figure 5. The generated trajectories illustrate that the five followers can successfully keep up with the leader, and avoid collisions between each other at the same time.

To further quantitatively evaluate the performance of the learned SEMP policy, we defined *collision rate* as a metric aside from the average reward. We considered that a collision would happen if the distance between two followers was less than a certain value, e.g., 5 meters. Thus, the *collision rate* meant the percentage of being too close (i.e., less than 5 meters) among the followers during the testing episode.

We compared the learned SEMP policy with three baselines by averaging the results of 200 experiments. In each experiment, the initial state of the leader and the followers were initialized randomly. The maximum time step ( $N_s$ ) for each episode was set to 180. At each time step, the steer commands of the leader were generated randomly. Table II and Figure 6 compares the results of the four methods.

In Table II,  $n$  denotes the number of the followers. As can be seen, the learned policies with one set of network parameters can adapt to a dynamic squad of UAVs, without the need of retraining in a new environment with different number of followers. When the number of followers increases, the average reward decreases and the collision rate increases. The reason is that increasing the number of followers leads to a higher probability of collision. However, compared with the other three baselines, our SEMP method enables the follower to obtain the largest average reward, the lowest collision rate, and the lowest variance, regardless of the number of followers. This result shows that the SEMP method outperforms the three existing state-of-the-art methods.

### C. Semi-Physical Simulation

In addition to the numerical simulation, we also tested the generalization performance of the learned control policy by conducting a hardware-in-loop (HIL) experiment in a high fidelity semi-physical simulation system [14], [15]. Instead of the kinematic model of fixed-wing UAVs with stochastic

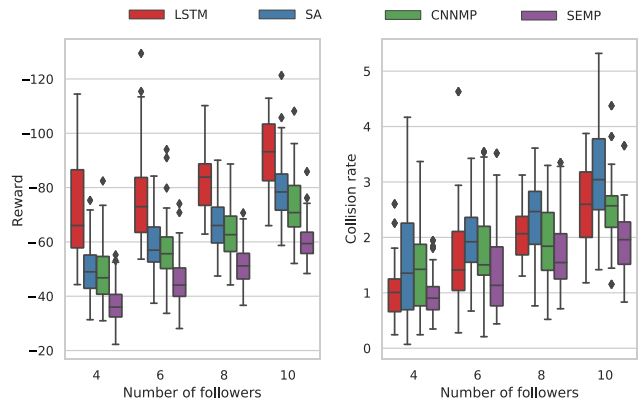


Fig. 6. Box-and-whisker plot for comparison results of LSTM, SA, CNNMP, and SEMP. **Left:** Reward. **Right:** Collision rate.

disturbances used in the training phase, we selected the professional tool X-Plane 10<sup>1</sup> as the flight simulator for the testing. X-Plane 10 can simulate complex environmental conditions, such as weather changes and wind disturbances.

In this experiment, the five followers used the learned SEMP policy to flock with the leader lasting for 200 time steps (seconds). At each time step, the leader selected its roll-angle setpoint according to the pre-planned paths and changed its velocity randomly, then broadcasted its state information to all the followers. Each follower used the actor network with the trained parameters to determine its steering commands according to its own state, the leader's state, and the other followers' states.

The trajectory results are depicted in Figure 7; the distances between the leader and the five followers ( $\rho$ ) as well as the minimum distance among the five followers ( $mindis$ ) are shown in Figure 8. As can be seen, the distances between the leader and the followers were maintained around 75 meters most of the time. This means that the five followers were able to keep up with the leader steadily, even if the leader changed its heading sharply. More importantly, the minimum value of  $mindis$  is larger than 5m, which means that there were no collisions among the followers during the experiment. The above results demonstrate that the proposed SEMP method enables the followers to avoid collisions between each other while flocking with the leader. We note that the control policy employed by the five followers in this semi-physical simulation is the SEMP policy learned from the previous

<sup>1</sup><https://www.x-plane.com/manuals/desktop/>

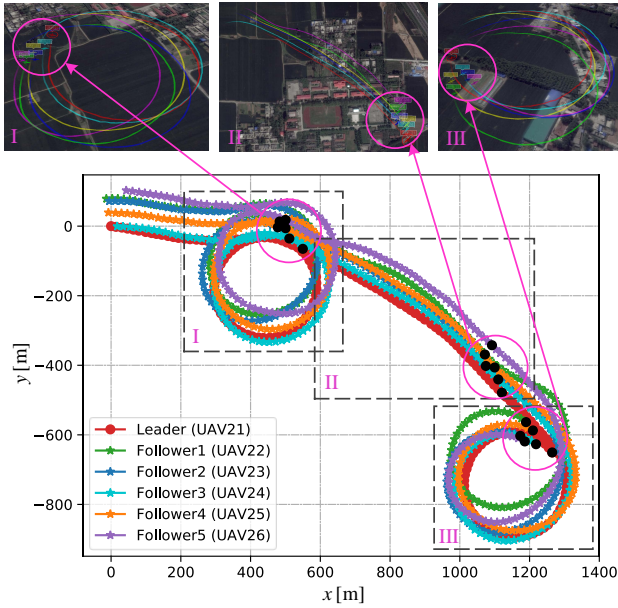


Fig. 7. The trajectory results in the semi-physical simulation. Note that the three representative snapshots displayed on the top are captured from the ground control station. The top-left and top-right snapshots show a third person perspective of the UAV flock, while the top-middle snapshot is top view.

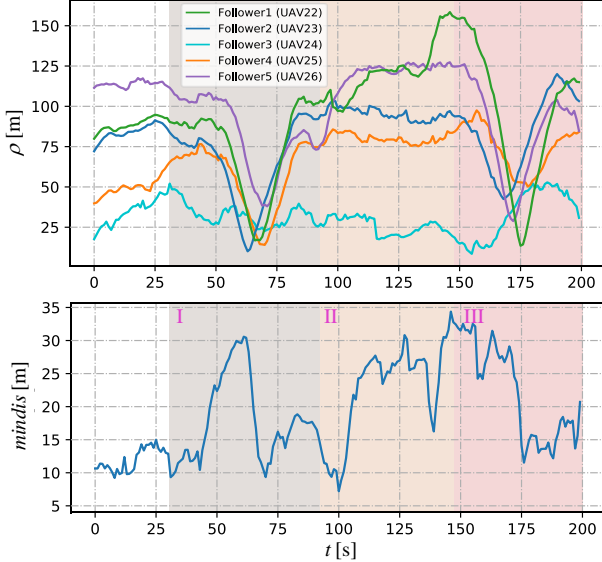


Fig. 8. The distances between the leader and five followers ( $\rho$ ) and the minimum distance among five followers ( $mindis$ ) in the semi-physical simulation.

numerical simulation, without any parameter finetuning. This result demonstrates that the learned SEMP policy can be directly generalized to new situations.

## V. CONCLUSION

In this paper, we have proposed a deep reinforcement learning algorithm to solve the collision-free leader-follower flocking control problem for a dynamic squad of fixed-wing

UAVs. Specifically, we have designed a decentralized DRL-based framework where the collision avoidance policy is integrated into the flocking controller for a variable number of UAVs. Then, we have proposed the CACER-II algorithm for training multiple agents, in which a customized embedding module, SEMP, is integrated to handle the variable-length input for deep neural networks. With this module, the learned policies are adaptive to the changes of the number of UAVs without the need of retraining. Numerical simulation results have demonstrated that the proposed method outperforms three existing state-of-the-art methods, i.e., LSTM, SA, and CNNMP. Finally, the learned policy can be directly transferred to a semi-physical simulation without any parameter finetuning. In the future, we will further evaluate our method with fixed-wing UAVs in real-world environments.

## REFERENCES

- [1] Y. Tang, Y. Hu, J. Cui, F. Liao, M. Lao, F. Lin, and R. S. Teo, "Vision-aided multi-UAV autonomous flocking in GPS-denied environment," *IEEE Transactions on Industrial Electronics*, vol. 66, no. 1, pp. 616-626, Jan. 2019.
- [2] C. H. Liu, X. Ma, X. Gao and J. Tang, "Distributed Energy-Efficient Multi-UAV Navigation for Long-Term Communication Coverage by Deep Reinforcement Learning," in *IEEE Transactions on Mobile Computing*, vol. 19, no. 6, pp. 1274-1285, 1 June 2020.
- [3] S. Chung, A. A. Paranjape, P. Dames, S. Shen, and V. Kumar, "A Survey on Aerial Swarm Robotics," *IEEE Transactions on Robotics*, vol. 34, no. 4, pp. 837-855, Aug. 2018.
- [4] Y. Kuriki, and T. Namerikawa, "Formation control with collision avoidance for a multi-UAV system using decentralized MPC and consensus-based control," in *European Control Conference (ECC)*, Linz, 2015, pp. 3079-3084.
- [5] O. Saif, I. Fantoni, and A. Zavala-Río, "Distributed integral control of multiple UAVs: precise flocking and navigation," *IET Control Theory & Applications*, vol. 13, no. 13, pp. 2008-2017, 2019.
- [6] R.S. Sutton, and A.G. Barto, *Reinforcement learning: An introduction*. Cambridge, USA: MIT Press, 1998.
- [7] C. Yan, and X. Xiang, "A path planning algorithm for UAV based on improved Q-learning," in *International Conference on Robotics and Automation Sciences (ICRAS)*, Wuhan, 2018, pp. 1-5.
- [8] S. Hung, S. N. Givigi, and A. Noureddin, "A Dyna-Q ( $\lambda$ ) approach to flocking with fixed-wing UAVs in a stochastic environment," in *IEEE International Conference on Systems, Man, and Cybernetics*, Kowloon, 2015, pp. 1918-1923.
- [9] S. Hung, and S. N. Givigi, "A Q-learning approach to flocking with UAVs in a stochastic environment," *IEEE Transactions on Cybernetics*, vol. 47, no. 1, pp. 186-197, Jan. 2017.
- [10] S. C. Speck, and D. J. Bucci, "Distributed UAV swarm formation control via object-focused, multi-objective SARSA," in *Annual American Control Conference (ACC)*, Milwaukee, WI, 2018, pp. 6596-6601.
- [11] C. Yan, X. Xiang, and C. Wang, "Towards Real-Time Path Planning through Deep Reinforcement Learning for a UAV in Dynamic Environments," *Journal of Intelligent & Robotic Systems*, vol. 98, no. 2, pp. 297-309, 2020.
- [12] L. Tai, G. Paolo, and M. Liu, "Virtual-to-real deep reinforcement learning: Continuous control of mobile robots for mapless navigation," in *IEEE/RSJ International Conference on Intelligent Robots and Systems (IROS)*, Vancouver, BC, 2017, pp. 31-36.
- [13] A. Singla, S. Padakandla, and S. Bhatnagar, "Memory-based deep reinforcement learning for obstacle avoidance in UAV with limited environment knowledge," *IEEE Transactions on Intelligent Transportation Systems*, 2019, In press, DOI: 10.1109/TITS.2019.2954952
- [14] C. Wang, C. Yan, X. Xiang, and H. Zhou, "A continuous actor-critic reinforcement learning approach to flocking with fixed-wing UAVs," in *Asian Conference on Machine Learning (ACML)*, Nagoya, Japan, 2019, pp. 64-79.
- [15] C. Yan, X. Xiang, and C. Wang, "Fixed-Wing UAVs flocking in continuous spaces: A Deep reinforcement learning approach," *Robotics and Autonomous Systems*, 2020, In press, DOI: 10.1016/j.robot.2020.103594

[16] Z. Sui, Z. Pu, J. Yi, and T. Xiong, "Formation control with collision avoidance through deep reinforcement learning," in *International Joint Conference on Neural Networks (IJCNN)*, Budapest, Hungary, 2019, pp. 1-8.

[17] M. Everett, Y. F. Chen, and J. P. How, "Motion planning among dynamic, decision-making agents with deep reinforcement learning," in *IEEE/RSJ International Conference on Intelligent Robots and Systems (IROS)*, Madrid, 2018, pp. 3052-3059.

[18] S. Hochreiter, and J. Schmidhuber, "Long short-term memory," *Neural Computation*, vol. 9, no. 8, pp. 1735-1780, 1997.

[19] C. Wang, J. Wang, and X. Zhang, "A deep reinforcement learning approach to flocking and navigation of UAVs in large-scale complex environments," in *IEEE Global Conference on Signal and Information Processing (GlobalSIP)*, Anaheim, CA, USA, 2018, pp. 1228-1232.

[20] C. Kownacki, D. Odziej, J. Bordeneuve-Guibé, A. Drouin, and C. Roos, "Flocking algorithm for fixed-wing unmanned aerial vehicles," in *Advances in Aerospace Guidance Navigation and Control*, Springer, pp. 415-431, 2015.

[21] Y. F. Chen, M. Liu, M. Everett, and J. P. How, "Decentralized non-communicating multiagent collision avoidance with deep reinforcement learning," in *IEEE International Conference on Robotics and Automation (ICRA)*, Singapore, 2017, pp. 285-292.

[22] T. Lillicrap, J. Hunt, A. Pritzel, N. Heess, T. Erez, Y. Tassa, D. Silver, and D. Wierstra, "Continuous control with deep reinforcement learning," in *International Conference on Learning Representations (ICLR)*, IEEE, 2016.

[23] X. B. Peng, G. Berseth, K. Yin, and M. Van De Panne, "DeepLoco: Dynamic locomotion skills using hierarchical deep reinforcement learning," *ACM Transactions on Graphics*, vol. 36, no. 4, pp. 1-13, 2017.

[24] H. van Hasselt, "Reinforcement learning in continuous state and action spaces," In *Reinforcement Learning*, Springer, 2012, pp. 207-251.

[25] K. G. Jayesh, E. Maxim, and K. Mykel, "Cooperative multi-agent control using deep reinforcement learning", in *International Conference on Autonomous Agents and Multiagent Systems (AAMAS)*, Cham, 2017, pp. 66-83.

[26] C. Hoel, K. Wolff, and L. Laine, "Automated speed and lane change decision making using deep reinforcement learning," in *International Conference on Intelligent Transportation Systems (ITSC)*, Maui, HI, 2018, pp. 2148-2155.

[27] J. Hu, L. Shen, and G. Sun, "Squeeze-and-excitation networks," in *IEEE Conference on Computer Vision and Pattern Recognition (CVPR)*, Salt Lake City, USA, 2018, pp. 7132-7141.

[28] D. P. Kingma and J. Ba, "Adam: A method for stochastic optimization," *arXiv preprint arXiv:1412.6980*, 2014.

[29] C. Chen, Y. Liu, S. Kreiss, and A. Alahi, "Crowd-robot interaction: Crowd-aware robot navigation with attention-based deep reinforcement learning," in *International Conference on Robotics and Automation (ICRA)*, Montreal, Canada, 2019, pp. 6015-6022.